

Influence of Wettability on Residual Gas Trapping and Enhanced Oil Recovery in Three-Phase Flow: a Pore-Scale Analysis using Micro-Computed Tomography*

S. Iglauer¹, M. Sarmadivaleh¹, M. Lebedev¹, and M. Ferno²

Search and Discovery Article #41353 (2014)

Posted May 12, 2014

*Adapted from extended abstract prepared in conjunction with oral or poster presentation at GEO-2014, 11th Middle East Geosciences Conference and Exhibition, 10-12 March 2014, GEO-2014©2014

¹Curtin University, Perth, Western Australia

²Bergen University, Bergen, Norway

Abstract

We imaged two enhanced oil recovery processes in a mixed-wet sandstone plug at high resolution ($3.4\mu\text{m}$)³ with a micro-computed tomograph. In the first process, gas was directly injected into an oil reservoir, which was subsequently waterflooded (S_{ogb} process). In the second process, the oil reservoir was first waterflooded, then gas-flooded and finally waterflooded again (S_{obgb} process – typically referred to as water-alternating-gas process). We qualitatively found that during immiscible gas/brine/oil displacements a) similar amounts of gas can be stored in a mixed-wet reservoir with the S_{ogb} and the S_{obgb} processes compared with the S_{ogb} process in a water-wet reservoir (note that less gas can be stored in a water-wet reservoir with the S_{ogb} process), and b) more oil can be produced with a S_{ogb} process compared to S_{obgb} in a mixed-wet reservoir, contrary to the situation in a water-wet reservoir, where the S_{ogb} process is more efficient. In addition, we identified several pore-scale fluid configurations, which ultimately determine reservoir flow properties.

Introduction

Three-phase (oil, gas and water) flow through rock is a phenomenon that frequently occurs in subsurface oil reservoirs when producing below the bubble point pressure. Such fluid pressure conditions may be given right from the start of production or may develop later on in the life of an oil field when sufficient oil volumes have been recovered so that the associated fluid pressure has been reduced sufficiently and a gas-oil phase separation is induced. In addition, analogue three phase flow can be relevant in contaminant transport in soil, where organic solvent or oil has been spilled into the vadose zone, and air, water and the organic phase form a three-phase fluid system.

It is therefore of vital importance to be able to predict the static and dynamic fluid configurations of such three-phase systems, so that oil recovery can be increased (e.g. compare Lake 2010, Blunt et al., 1993, Iglauer et al., 2013) or organic contaminants can be removed efficiently from soil (e.g. Sleep and McClure 2001).

Routinely these processes are predicted with reservoir simulators at the hectometre scale (e.g. Qi et al., 2009, Moortgat et al., 2011). These simulators, however, require input parameters: capillary pressure curves, relative permeabilities and residual saturations; and these parameters can be measured in laboratory experiments (e.g. Dumoré and Schols 1997, Oak et al., 1990, Al-Mansoori et. al, 2009) or they can be computed with pore-network models (e.g. Soll et al., 1993, Dong and Blunt 2009, Pentland et al., 2010). As laboratory experiments are time-consuming and expensive, a modeling approach to acquire the required parameters is often the choice in research and particularly industrial projects. The problem with the pore-scale models is, however, that they are built on scant physical data and they need to be verified to a better degree or possibly upgraded to respect the underlying physical phenomena.

Apart from theoretical work where pore-scale fluid configurations were derived from force balances (Piri and Blunt 2004), several researchers studied three-phase fluid systems in 2D micromodel experiments (e.g. Oren et al., 1992, Oren and Pinczewski 1995, Dong et al., 1995, Keller et al., 1997). Despite very interesting insights into the exact fluid configurations and flow behaviour at the micrometre pore-scale, it is well established that 3D flow characteristics cannot be fully captured using 2D models (e.g. the percolation threshold in 3D is significantly lower than in 2D, Stauffer 1979). Only recently, with the advent of micro-computed tomography (μ CT), these phenomena can be studied in 3D at the pore-scale (compare the recent reviews by Blunt et al. (2013) and Wildenschild and Sheppard (2013)), which is most relevant for industrial applications.

In the work we present here, we add more hard data to the global database in this area, and we focus on one important factor, which is known to have a dramatic effect on pore-scale fluid configurations, but has received little attention so far in the area of three-phase 3D flow through porous media investigations: wettability. This work is essentially an extension of a previous study (Iglauer et al. 2013), where we examined such fluid configurations in a water-wet sandstone. We now studied a mixed-wet sandstone system, and this is of particular importance for oil reservoirs, which are well known to be not necessarily water-wet, but instead can be mixed-wet or oil-wet (Cuiec 1991). And it is also well established that such a shift in wettability has a significant effect on relative permeabilities (e.g. McCaffery and Bennion 1974), residual saturations (e.g. Morrow 1990, Iglauer et al., 2012, Tanino and Blunt 2012) and capillary pressures (Anderson 1987), but as mentioned above the detailed pore-scale physics are still poorly understood and need to be improved. We therefore now present our μ CT analysis of oil, gas and water pore-scale configurations in a mixed-wet plug and discuss differences in fluid topologies when compared to an analogue water-wet plug.

Experimental Methodology

We selected a clean homogenous water-wet outcrop sandstone (Clashach, from Elgin in Scotland) with a porosity of 14.4% (Pentland et al., 2012) and a brine permeability of $9.6 \times 10^{-14} \text{ m}^2$ (Iglauer et al. 2012) for our study; its chemical composition was measured via XRD (96wt% quartz, 2wt% K-feldspar, 1wt% calcite, 1wt% ankerite and illite traces). From a larger block we drilled a small cylindrical plug (5mm diameter, 9mm length) and altered its wettability with North Sea crude oil using a procedure described previously (Iglauer et al. 2012) to mixed-wet (Amott-Harvey index = -0.1, Amott oil index = -0.1, and Amott water index = 0; which is slightly oil-wet). The aged plug (now housed in a flow cell) was then imaged with a micro-computed tomograph (Xradia Versa-XRM-T500) at a resolution of $(3.4 \mu\text{m})^3$. Note that an inner cylindrical volume of the plug was imaged with a diameter of 3.4mm to achieve good resolution (i.e. not the whole 5mm-diameter plug). The same resolution was used throughout the whole workflow for each μ CT scan. The plug was then vacuumed for at least 60min and deaired brine

was injected for at least 5 min under vacuum followed by injection of ~ 1000 PV of oil at a capillary number ($\mu q/\gamma$, where q is the Darcy flow rate, μ is the viscosity of the injected phase and γ is the interfacial tension) of 3.54×10^{-4} to achieve connate water saturation S_o . The brine was a 10wt% solution of potassium iodide (KI) in deionized water; the KI is required to achieve sufficient x-ray contrast between the fluids. The oil used was 1-bromododecane (purity ≥ 99 mol%, from Sigma Aldrich), again to enable CT contrast. The plug then essentially represented an oil reservoir (“connate water saturation”, with no gas present), and we acquired a μ CT image of the plug in this state. Following our previous study line, we then distinguished two cases:

1. We flooded the plug at connate water saturation with 25 PV of brine at a capillary number of 7.4×10^{-7} to establish residual oil saturation (S_{ob}), and this state was again imaged. Subsequently, approximately 50 PV of N_2 gas were injected into the plug at S_{ob} at a pressure drop of 20,000 Pa over a 9mm plug length (0.05 mL/min flow rate for six minutes), which approximately corresponds to a capillary number of 0.01, so that an initial gas saturation state (S_{obg}) was established. The pore pressure was atmospheric. This state was imaged, and another brine flood was performed (using the same capillary number) to test residual oil and gas saturations and configurations (S_{obgb} state) by imaging the plug again.
2. In an independent experiment, a second workflow was applied: N_2 gas was directly injected into the same plug at connate water saturation (S_o) using the same conditions as above and then imaged again at initial gas saturation, S_{og} . This was followed by brine injection (same conditions as above) to establish residual gas saturation, S_{ogb} , which was then also imaged.

Flow scheme 1 resembles the process typically used in the oil and gas industry, where oil reservoirs are waterflooded to enhance oil recovery, and subsequently gas flooded for further improving oil recovery (e.g. Iglauer et al., 2010) and/or gas storage (e.g. CO_2 storage, cp. e.g. Iglauer et al., 2011a, Iglauer et al. 2013, Pentland et al. 2012), i.e. the WAG flood. The second flow scheme uses an alternative process sequence, which has been shown to be significantly more efficient in terms of oil recovery and gas storage in a water-wet plug (Iglauer et al. 2013). All experiments were conducted at ambient laboratory conditions, that are 295K and 0.1MPa, and the plugs were always positioned horizontally during the floods. Bond numbers were estimated to be $\approx 10^{-5}$ for the liquid-gas system and 10^{-7} for the oil-brine system; we therefore do not expect the residual clusters/residual saturations to be influenced by buoyancy forces (Morrow et al. 1988).

We note that the oil used was non-spreading with a spreading coefficient S ($= \gamma_{gw} - \gamma_{ow} - \gamma_{go}$, where γ_{gw} is the gas-brine interfacial tension, γ_{ow} is the oil-brine interfacial tension and γ_{go} is the gas-oil interfacial tension, cp. [Table 1](#)) of -11.05 mN/m. The algebraic sign of S has a profound influence of the fluid dynamics and statics (Blunt et al., 1995, Oren et al. 1995).

Results and Discussion

[Figure 1](#) shows a set of 2D slices through the rock and pore space filled with fluids at different saturation stages: connate water saturation (S_o), residual oil saturation (S_{ob}), the two initial gas saturations (S_{og} and S_{obg}), and the two residual gas saturations (S_{ogb} and S_{obgb}). The slices display a greyscale map, where each greyscale corresponds to a specific relative radiodensity of a volume element, and this greyscale can be assigned to a certain material (i.e. rock, oil, gas or water). The gas has the lowest relative radiodensity and it is thus black, while oil (because it is

brominated) has the highest relative radiodensity: it is white. The brine and the solid grains have a relative radiodensity in between, they are both grey; the brine being slightly darker than the grains (except in the S_o and S_{ob} states where it is black).

[Figure 2](#) displays the influence of wettability (water-wet versus mixed-wet) on the two residual gas saturation states (S_{ogb} and S_{obgb}). Note that the tomograms of the water-wet plugs have been acquired earlier with synchrotron radiation at a nominal resolution of $(9\mu\text{m})^3$ (Iglauer et al. 2013). For the mixed-wet plug, it appears that qualitatively the S_{obgb} flooding process is more efficient in terms of oil recovery (i.e. more oil is produced) than the alternative S_{ogb} technique. The oil in the S_{obgb} sequence has accumulated in small oil banks, and the oil has been mobilised more into the centres of the pores, probably after the first waterflood – as the oil distribution changes are similar to those observed when waterflooding a mixed-wet plug at connate water saturation (cp. [Figure 1 a and b](#)); this is contrary to the situation in a water-wet plug (Iglauer et al. 2013), however, the data presented here needs to be quantified so that a high-confidence conclusion can be reached about this phenomenon.

Furthermore, it appears qualitatively that substantial amounts of gas can be stored in mixed-wet rock using both flooding sequences: S_{ogb} and S_{obgb} (this is of particular importance in the context of CO_2 storage, Iglauer et al. 2011b). This is again contrary to the situation in water-wet sandstone, where significantly more gas can be stored using the S_{ogb} process (Iglauer et al. 2013) – but as above these datasets need to be re-evaluated in the light of the additional quantitative information, which is currently being processed.

Pore-Scale Fluid Configuration

[Figure 3](#) shows the zoom-ins on some selected slice areas, and the pore scale configuration of the different fluid phases can be quite clearly seen. As expected, the gas, the non-wetting phase, occupies the centres of the larger pore bodies because of capillary forces (e.g. Øren and Pinczewski, 1995). The oil – contrary to the water-wet rock case, where the oil is intermediate wet and sandwiched between the gas and the water phase (Iglauer et al. 2013) – is quasi randomly distributed in all pores (except the largest pores where gas has displaced the initial phase). This is consistent with the mixed-wet character of the rock.

The gas clusters can take a range of morphologies: from spherical to ganglia-like, the specific morphology and its associated surface curvature C are related by differences in the capillary pressures pc , equation (1):

$$pc=C\gamma \tag{1}$$

This type of behaviour for a non-wetting phase is consistent with what has been observed earlier (Prodanovic et al., 2007, Iglauer et al. 2010, 2011, 2012, 2013, Pentland et al. 2012). As a next step in our analysis, we identified a number of pore scale fluid configurations; a summary is tabulated in [Table 2](#). Some of these configurations have been theoretically predicted (Piri and Blunt 2004).

Conclusions

We have imaged two enhanced oil recovery process sequences with a micro-computed tomograph at a nominal resolution of $(3.4\mu\text{m})^3$: in the first process gas was directly injected into a simulated mixed-wet oil reservoir and then waterflooded (S_{ogb} process), while in the second process the mixed-wet oil reservoir was first waterflooded, then gasflooded and waterflooded again (S_{obgb} process). Qualitatively, and contrary

to a water-wet reservoir previously studied by us, more oil could be recovered via the S_{ogb} process. However, again based on a qualitative assessment, with both processes, similar amounts of gas can be stored in a mixed-wet reservoir. This is also contrary to the situation in a water-wet reservoir, where significantly more gas can be stored using the S_{ogb} process. Moreover, we investigated the exact pore-scale fluid distributions and we observed several fluid configurations, which were previously predicted theoretically.

Acknowledgements

We would like to thank the National Geo-sequestration Laboratory for providing access to the microCT scanner.

References Cited

Anderson, W.G., 1987, Wettability Literature Survey- Part 4: The Effects of Wettability on Capillary Pressure: Journal of Petroleum Technology, v. 39/10, p. 1283–1300.

Al-Mansoori, S.K., S. Iglauer, C.H. Pentland, and M.J. Blunt, 2009, Three-phase measurements of oil and gas trapping in sand packs: Advances in Water Resources., v. 32, p. 1535-1542.

Blunt, M.J., F.J. Fayers, and F.M. Orr, 1993, Carbon dioxide in enhanced oil recovery: Energy Conversion and Management, v. 34, p. 1197-1204.

Blunt, M.J., B. Bijeljic, H. Dong, O. Gharbi, S. Iglauer, P. Mostaghimi, A. Paluszny, and C. Pentland, 2013, Pore-scale imaging and modelling: Advances in Water Resource, v. 51, p. 197-216.

Blunt, M.J., D. Zhou, and D. Fenwick, 1995, Three-phase flow and gravity drainage in porous media: Transport in Porous Media, v. 20, p. 77-103.

Cuiec, L.E., 1991, Evaluation of reservoir wettability and its effect on oil recovery. In: Interfacial Phenomena in Petroleum Recovery (ed.: N.R. Morrow). New York, 462 p.

Dong, M. F.A.L. Dullien, and I. Chatzis, 1995, Imbibition of oil in film form over water present in edges of capillaries with an angular cross section: J. Colloid Interf Sci., v. 172, p. 21-36.

Dong, H., and M.J. Blunt, 2009, Pore-network extraction from micro-computerized tomography images: Physical Review E., v. 80, 036307.

Dumoré, J.M., and R.S. Schols, 1997, Drainage capillary-pressure functions and the influence of connate water: *SPE J.* p. 437-444.

Iglauer, S., S. Favretto, G. Spinelli, G. Schena, and M.J. Blunt, 2010, X-ray tomography measurements of power-law cluster size distributions for the nonwetting phase in sandstones: *Physical Review E.*, v. 82, 056315.

Iglauer, S., A. Paluszny, C.H. Pentland, and M.J. Blunt, 2011a, Residual CO₂ imaged with X-ray micro-tomography: *Geophysical Research Letters*, v. 38/21, L21403.

Iglauer, S., W. Wuelling, C.H. Pentland, S.K. Al-Mansoori, and M.J. Blunt, 2011b, Capillary-trapping capacity of sandstones and sandpacks: *SPE Journal*, v. 16/4, p. 778-783.

Iglauer, S., M.A. Fernø, P. Shearing, and M.J. Blunt, 2012, Comparison of residual oil cluster size distribution, morphology and saturation in oil-wet and water-wet sandstone: *Journal of Colloid and Interface Science*, v. 375/1, p. 187-192.

Iglauer, S., A. Paluszny, and M. Blunt, 2013, Simultaneous oil recovery and residual gas storage: a pore-level analysis using in-situ x-ray micro-tomography: *Fuel*, v. 1, p. 1-11.

Keller, A.A., M.J. Blunt, and P.V. Roberts, 1997, Micromodel observation of the role of oil layers in three-phase flow: *Transport Porous Med.*, v. 26, p. 277-297.

Lake, L.W., 2010, *Enhanced Oil Recovery*, Richardson: SPE Publications.

McCaffery, F.G., and D.W. Bennion, 1974, The effect of wettability on two phase relative Permeabilities: *Journal of Canadian Petroleum Engineering*, v. 13/4, p. 42-53.

Moortgat, J., S. Sun, and A. Firoozabadi, 2011, Compositional modelling of three-phase flow with gravity using higher-order finite element methods: *Water Resources Research*, v. 47, W05511.

Morrow, N., I. Chatzis, and J. Taber, 1988 Entrapment and mobilization of residual oil in bead packs: *SPE Reservoir Engineering*, v. 3, p. 927-934.

Morrow, N.R., 1990, Wettability and Its Effect on Oil Recovery: *Journal of Petroleum Technology*, v. 42/12, p. 1476-1484.

Oak, M.J., L.E. Baker, and D.C. Thomas, 1990, Three-phase relative permeability of Berea sandstone: *Journal of Petroleum Technology*, v. 42, p. 1054-1061.

Oren, P.E., J. Billiote, and W.V. Pinczewski, 1992, Mobilization of waterflood residual oil by gas injection for water-wet conditions: *SPE Form Eval.*, v. 7, p. 70-78.

Oren, P.E., and W.V. Pinczewski, 1995, Fluid distribution and pore-scale displacement mechanisms in drainage dominated three phase flow. *Transport Porous Med.*, v. 20, p. 105-133.

Pentland, C.H., Y. Tanino, S. Iglauer, and M.J. Blunt, 2010, Capillary trapping in water-wet sandstone: coreflooding experiments and pore-network modelling: *SPE Annual Tech Conf 2010*, SPE 133798.

Pentland, C., S. Iglauer, O. Gharbi, K. Okada, and T. Suekane, 2012, The Influence of Pore Space Geometry on the Entrapment of Carbon Dioxide by Capillary Forces, SPE 158516, *SPE Asia Pacific Oil and Gas Conference and Exhibition*, Perth, Australia.

Prodanovic, M., W. B. Lindquist, and R.S. Seright, 2007, 3D image-based characterization of fluid displacement in a Berea core: *Advances in Water Resources*, v. 30, p. 214–226.

Qi, R., T.C. LaForce, and M.J. Blunt, 2009, A three-phase four-component streamline-based simulator to study carbon dioxide storage: *Comput Geosci.*, v. 13, p. 493-509.

Piri, M., and M.J. Blunt, (2004, Three-phase capillary pressures in noncircular capillary tubes with different wettabilities including contact angle hysteresis: *Physical Review E.*, v. 70, 061603.

Sleep, B.E., and P.D. McClure, 2001, Removal of volatile and semivolatile organic contamination from soil by air and steam flushing: *Journal of Contaminant Hydrology*, v. 50, p. 21-40.

Soll, W.E., M.A. Celia, and J.L. Wilson, 1993, Micromodel studies of three-fluid porous media systems: pore-scale processes relating to capillary pressure-saturation relationships: *Water Resour Res.*, v. 29, p. 2963-2974.

Stauffer, D., 1979, Scaling theory of percolation clusters: *Phys Rep.*, v. 54, p. 1-74.

Tanino, Y., and M.J. Blunt, 2013, Laboratory investigation of capillary trapping under mixed-wet conditions: *Water Resources Research*, v. 49, 7, p. 4311–4319.

Wildenschild, D., and A.P. Sheppard, 2013, X-ray imaging and analysis techniques for quantifying pore-scale structure and processes in subsurface porous medium systems: *Advances in Water Resources*, v. 51, p. 217–246.

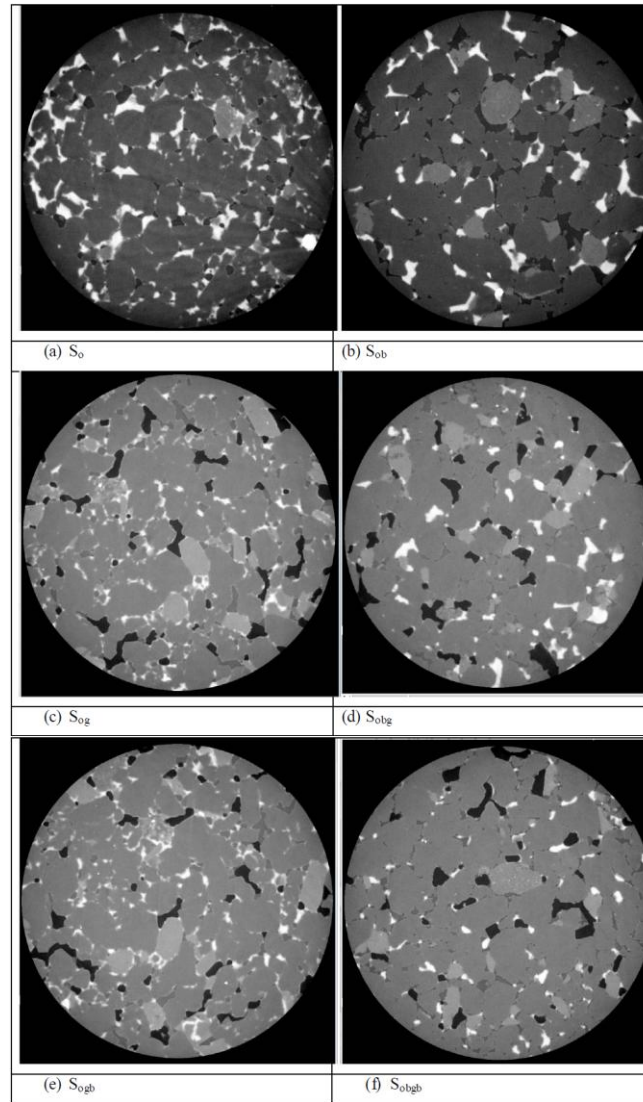


Figure 1. 2D slices through the rock and fluids at different saturation states. (a) S_o : connate water saturation: oil is white, brine is black, and sandstone is dark grey. (b) S_{ob} : residual oil saturation: oil is white, brine is black, and sandstone is dark grey. (c) S_{og} : initial gas saturation: oil is white, gas is black, brine dark grey and sandstone is light grey. (d) S_{obg} : initial gas saturation: oil is white, gas is black, brine dark grey and sandstone is light grey. (e) S_{ogb} : residual gas saturation: oil is white, gas is black, brine dark grey and sandstone is light grey; (f) S_{obgb} : residual gas saturation: oil is white, gas is black, brine dark grey and sandstone is light grey. The circles (plugs) shown in all slices have a diameter of 3.4mm.

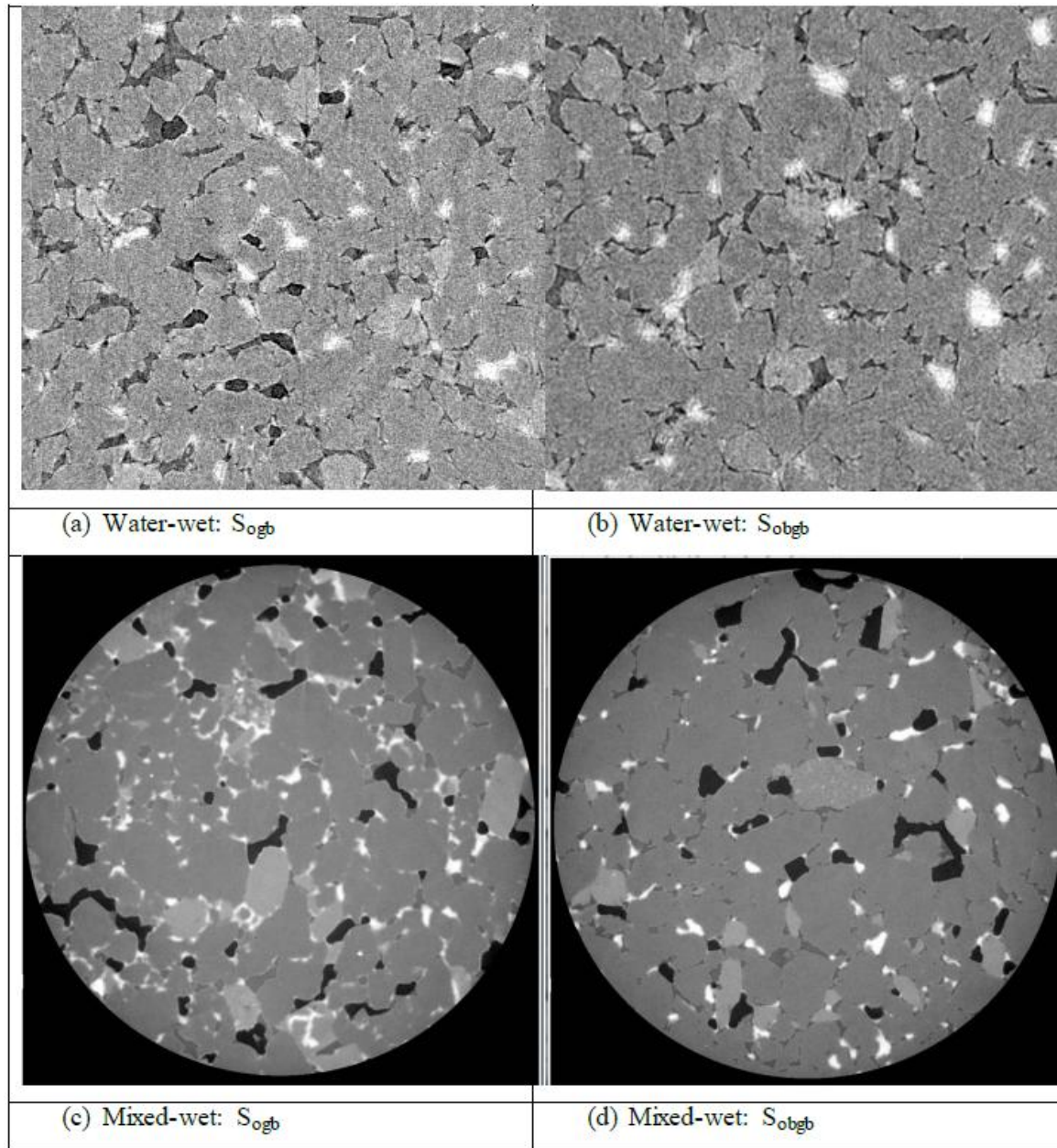


Figure 2. Comparison of fluid configurations at the two residual gas saturation states (S_{ogb} and S_{obgb}) in water-wet and mixed-wet plugs. Figures (a) and (b) show an area of $(2.7\text{mm})^2$, and Figures (c) and (d) show a circle with a diameter of 3.4mm.

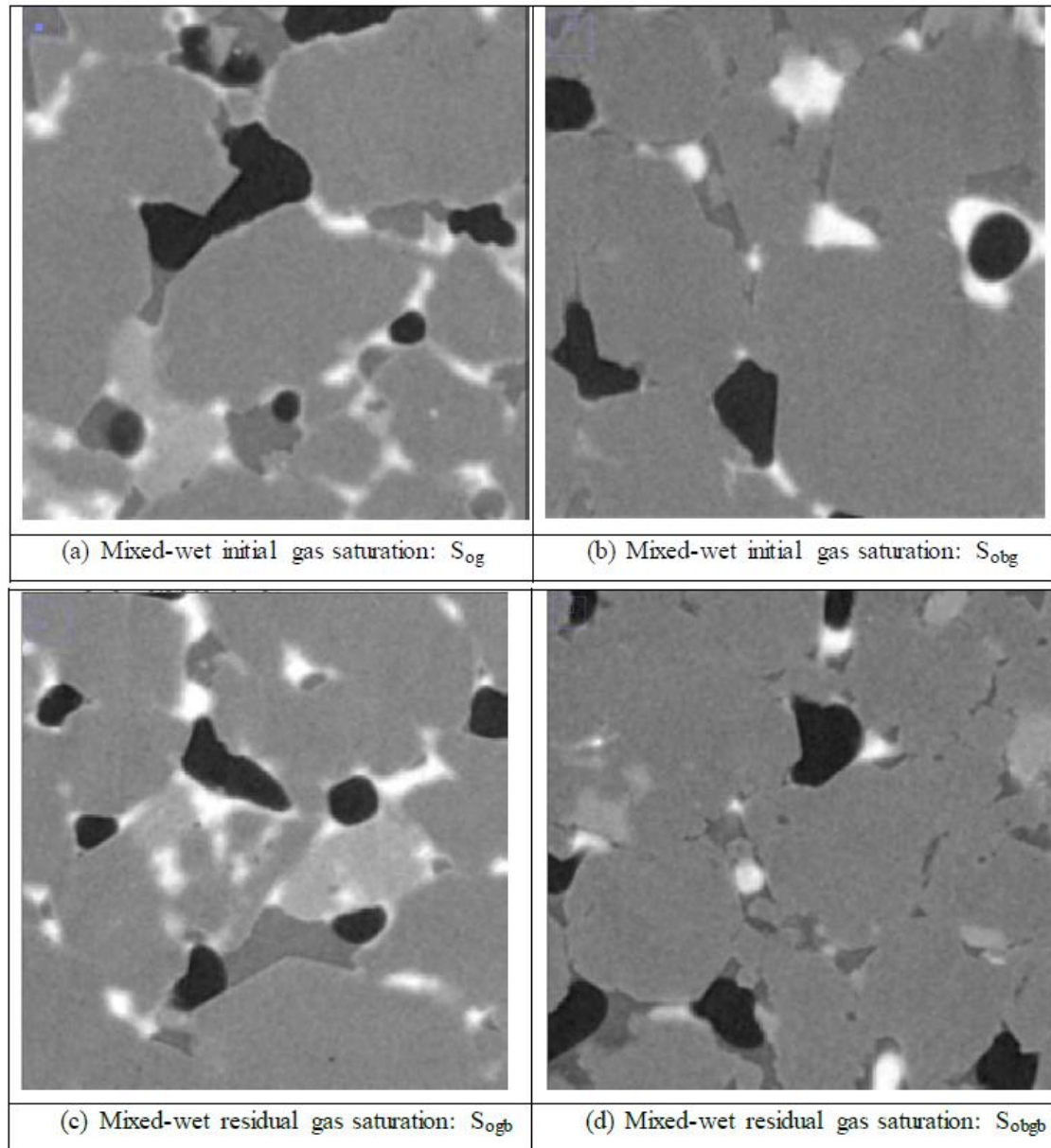


Figure 3. Zoom-ins on some selected μ CT slices of the mixed-wet plug; a comparison and analysis of pore-scale fluid configurations is possible: (a) initial gas saturation (S_{og}), (b) initial gas saturation (S_{obg}), (c) residual gas saturation (S_{ogb}) and (d) residual gas saturation (S_{obgb}). All areas shown are 250×250 pixels = $(850\mu\text{m})^2$. In the above slices gas is black, oil white, brine dark grey and rock light grey.

fluid-fluid system	interfacial tension [mN/m]
water/1-bromododecane [*]	$\gamma_{ow} = 52.09$
water/nitrogen ^{**}	$\gamma_{gw} = 72$
1-bromododecane/nitrogen ^{***}	$\gamma_{go} = 30.96$

^{*} measured at 295K (Ortiz-Arango and Kantzas 2009).

^{**} measured at 293.15K and 0.101 MPa (Lide 2007).

^{***} surface tension of 1-bromododecane.

Table 1. Interfacial tensions of the fluids used.


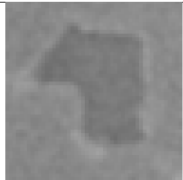



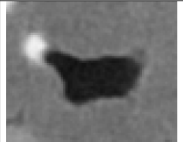

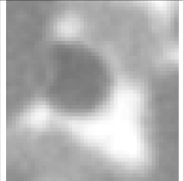

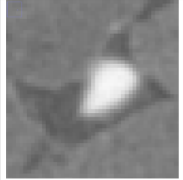

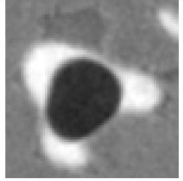

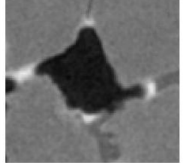
Pore-scale configuration		Pore-scale slice: zoom-in
	Water	
	Oil	
	Gas in oil or water	
	Water in oil	
	Oil in water	
	Gas in oil in water	
	Gas with oil layer in water	

Table 2. Pore-scale fluid configurations identified in the μ CT images of the mixed-wet plugs.